A Phase-Parameterized Frank-Sequence-Based CAZAC Waveform for Doubly Selective Channels

Zhuangzhuang Liao*†, Zunqi Li*, Yong Li‡, Xiaojie Fang*, Xuejun Sha*, and Dirk Slock†
*Harbin Institute of Technology, Harbin, China
†Communication Systems Department, Eurecom, Biot, France
‡National Key Laboratory of Advanced Communication Networks, Shijiazhuang, Hebei, China
Email: {Liao.Zhuangzhuang, Dirk.Slock}@eurecom.fr, lizunqi@stu.hit.edu.cn,
young_li_54@126.com, {fangxiaojie, shaxuejun}@hit.edu.cn

***Abstract*—Reliable communications over doubly selective channels require waveforms that are robust to both delay and Doppler spreads while maintaining low-complexity reception. Constant-amplitude zero autocorrelation (CAZAC) sequences provide attractive correlation properties and implementation advantages, yet their direct use in doubly selective channels is often suboptimal due to limited design flexibility. In this paper, we propose a phase-parameterized Frank sequence construction that preserves the CAZAC property while introducing an additional phase-parameter vector. Building on this construction, we develop a CAZAC waveform family tailored to doubly selective channels and propose two associated orthogonal modulation schemes. Compared with the fixed-structure Frank-sequence-based construction, the proposed waveform family can provide improved error-rate performance under doubly selective fading. Furthermore, simulation results show that, with linear MMSE reception, the proposed waveform achieves BER performance comparable to two representative high-mobility waveforms, namely, OTFS and AFDM. More importantly, in high-Doppler regimes, when combined with an MMSE-initialized iterative maximum-ratio combining (MRC) receiver, the proposed waveform provides a clear performance gain over OTFS and AFDM, indicating its suitability for high-mobility links.**

***Index Terms*—Frank sequence, CAZAC, doubly selective channels, iterative MRC**

I. Introduction

Emerging mobile communication scenarios, such as high-speed railways, vehicular networks, and low-altitude aerial links, increasingly demand reliable transmission under high mobility. In these regimes, the wireless channel exhibits both significant delay spread and fast time variation, i.e., a doubly selective channel [1]. Conventional orthogonal frequency division multiplexing (OFDM) and single-carrier frequency-domain equalization (SC-FDE), while mature and hardware-friendly, may suffer significant performance degradation when the joint delay-Doppler dispersion becomes severe.

To address high-mobility impairments from a more fundamental perspective, orthogonal time-frequency space (OTFS) modulation has been proposed as a delay-Doppler-domain waveform that maps information symbols onto a two-dimensional grid and exploits the compact structure of doubly selective channels [2]. By leveraging appropriate transforms between the delay-Doppler, time-frequency, and time domains, OTFS aims to convert the rapidly time-varying channel into a more stable and predictable effective representation over a packet duration [3].

Another recently proposed and actively studied waveform is affine frequency division multiplexing (AFDM), which builds on parameterized chirp signals and corresponding unitary transforms to provide flexible delay-Doppler coupling [4]. With properly selected chirp parameters, AFDM can achieve strong equalization robustness under linear minimum mean-square error (MMSE) reception and yield favorable error-rate performance [5]. From a broader perspective, AFDM can be interpreted as an extension of OFDM toward chirp-domain signaling, where appropriate parameter choices reduce to related chirp-based multicarrier structures, such as orthogonal chirp division multiplexing (OCDM) [6], and recent overviews highlight its flexibility across scenarios for beyond-5G highly dynamic links [7].

Beyond OTFS and AFDM, constant-amplitude zero autocorrelation (CAZAC) sequences provide an attractive building block due to their constant modulus and ideal cyclic autocorrelation properties, which often translate into implementation advantages and statistical robustness. Classical polyphase code families, such as the Frank sequence and the Chu sequence, exemplify such correlation-optimal constructions [8], [9]. However, directly using CAZAC sequences as communication waveforms in doubly selective channels does not always deliver the expected performance benefits.

In this paper, we study Frank-sequence-based CAZAC waveform construction and show that the conventional fixed-structure Frank (FS-Frank) design can be suboptimal in doubly selective fading due to its fixed coupling pattern. To address this issue, we consider a phase-parameterized Frank (PP-Frank) construction by introducing a vector of designable phases, which preserves the CAZAC property while providing additional design flexibility. Unlike AFDM, whose waveform flexibility is introduced through chirp parameterization, the adopted PP-Frank construction enlarges the Frank-sequence family by introducing phase degrees of freedom within the CAZAC class. Building on the PP-Frank construction, we develop a CAZAC waveform family tailored to doubly selective channels and propose two associated orthogonal modulation schemes. Compared with the FS-Frank baseline, the proposed waveform family yields improved error-rate performance under doubly selective fading. Furthermore, simulation results show that, with linear MMSE reception, the proposed waveform achieves BER performance comparable to two representative high-mobility waveforms, namely, OTFS and AFDM. More importantly, in high-Doppler regimes, when combined with an MMSE-initialized iterative maximum-ratio combining (MRC) receiver, the proposed waveform provides a clear performance gain over OTFS and AFDM, indicating its suitability for high-mobility doubly selective links.

II. PP-Frank-Based Waveform Design

A. PP-Frank Sequence Construction

A length-N complex sequence $\{c(n)\}_{n=0}^{N-1}$ is said to be a CAZAC sequence if it satisfies: (i) constant amplitude $|c(n)| = \mathrm{const}$ for all n, and (ii) zero cyclic autocorrelation

$$R_c(\ell) = \sum_{n=0}^{N-1} c(n)\, c^*(n-\ell) = 0, \qquad \forall\, \ell \not\equiv 0 \ (\mathrm{mod}\ N). \quad (1)$$

The CAZAC property makes such sequences attractive waveform prototypes, since both the sequence and its DFT have constant modulus. This structural feature is useful for waveform construction and implementation, and therefore makes CAZAC sequences a natural starting point for modulation design in doubly selective channels.

AFDM employs a chirp-based signal as its fundamental building block, which can be expressed as

$$c(n) = \exp\left(-\frac{j\pi u n^2}{N}\right), \quad n = 0, 1, \ldots, N-1, \quad (2)$$

where N denotes the signal length and u is an integer parameter. When N is even and u is coprime with N, (2) reduces to a Zadoff-Chu (ZC) sequence of even length, which is known to possess the CAZAC property.

Another class of sequences exhibiting the CAZAC property is the Frank sequence. An FS-Frank sequence is constructed based on an $M \times M$ square matrix, resulting in a sequence length $N = M^2$. The phase of the (p, q)-th element is given by

$$\phi_{p,q} = \frac{2\pi}{M}(p \cdot q), \quad (3)$$

where $p, q \in \{0, 1, \ldots, M-1\}$, and the corresponding one-dimensional index is $n = pM + q$. The resulting complex-valued sequence can be written as

$$c(n) = e^{j\frac{2\pi}{M}(p\cdot q)}. \quad (4)$$

The FS-Frank sequence construction is equivalent to the row-wise vectorization of the transpose of an $M \times M$ discrete Fourier transform (DFT) matrix, i.e.,

$$\mathbf{c}_{\mathrm{FS-Frank}} = \mathrm{vec}_{\mathrm{row}}\left(\mathbf{F}_M^{\mathrm{T}}\right), \quad (5)$$

where $\mathbf{F}_M$ denotes the $M \times M$ DFT matrix.

Although the FS-Frank sequence is CAZAC, its direct use in doubly selective channels is often suboptimal in terms of error-rate performance. This observation does not undermine the usefulness of the CAZAC property. Rather, it indicates that CAZAC alone is insufficient to guarantee favorable performance in doubly selective channels. In particular, the fixed and non-adjustable time-frequency coupling structure of the FS-Frank sequence may interact unfavorably with channel-induced delay-Doppler dispersion.

To address this issue, we consider a phase-parameterized extension of the FS-Frank sequence by introducing a vector of designable phases, which preserves the CAZAC property while providing additional design flexibility. Specifically, (5) is generalized as

$$\mathbf{c}_{\mathrm{Frank}} = \mathrm{vec}_{\mathrm{row}}\left((\mathbf{F}_M \mathbf{\Lambda})^{\mathrm{T}}\right), \quad (6)$$

where $\mathbf{\Lambda} = \mathrm{diag}\left(e^{j\theta}\right)$ is a diagonal matrix whose entries correspond to arbitrary initial phases applied to each DFT frequency component. The FS-Frank sequence in (5) is recovered by setting $\theta = \mathbf{0}$ (equivalently, $\mathbf{\Lambda} = \mathbf{I}_M$).

The unit-modulus construction immediately guarantees constant amplitude. To build intuition, note that (6) can be interpreted as an interleaving of M discrete tones (indexed by $k = 0, \ldots, M-1$), where each tone is upsampled by a factor of M (i.e., inserting $M-1$ zeros between adjacent samples). The N-point DFT of an upsampled tone becomes a periodically repeated spectral line pattern, and the M different tones occupy mutually non-overlapping DFT bins. Therefore, their superposition does not create inter-bin interference, and the DFT magnitude remains constant. The phase vector θ simply applies an arbitrary initial phase to each tone, which changes only the DFT phases but does not affect the constant-modulus conclusion due to tone orthogonality. Thus, the sequence constructed in (6) satisfies the CAZAC property for any choice of θ.

It is worth emphasizing that the CAZAC property remains the structural foundation of the proposed design. It guarantees constant modulus and enables the orthogonal waveform constructions used in this paper. However, CAZAC alone is not sufficient to ensure favorable performance in doubly selective channels. The proposed parameterized construction preserves the CAZAC backbone while introducing additional degrees of freedom to reshape the effective waveform-channel coupling.

B. Orthogonal Modulation Based on the PP-Frank Sequence

Owing to the zero cyclic autocorrelation of CAZAC sequences, it is straightforward to construct an orthogonal modulation scheme based on the PP-Frank sequence. In the following, we present two realizations: a *cyclic-shift realization* based on cyclic shifts, and a *frequency-shift realization* based on discrete frequency shifts.

1) Cyclic-Shift Realization (Cyclic-Shift Modulation): Let $\mathbf{c}_{\mathrm{Frank}} \in \mathbb{C}^{N\times 1}$ denote the proposed PP-Frank-based CAZAC waveform of length N. By taking all cyclic shifts of $\mathbf{c}_{\mathrm{Frank}}$ as columns, we form the circulant matrix $\mathbf{P}_t \in \mathbb{C}^{N\times N}$, i.e.,

$$\mathbf{P}_t = \left[\mathbf{c}_{\mathrm{Frank}},\ \mathbf{T}\mathbf{c}_{\mathrm{Frank}},\ \ldots,\ \mathbf{T}^{N-1}\mathbf{c}_{\mathrm{Frank}}\right], \quad (7)$$

where $\mathbf{T}$ denotes the $N \times N$ cyclic down-shift operator. Since $\mathbf{c}_{\mathrm{Frank}}$ is CAZAC, different cyclic shifts are orthogonal and have identical norms. With proper normalization, we have $\mathbf{P}_t^{\mathrm{H}}\mathbf{P}_t = \mathbf{I}_N$.

Using $\mathbf{P}_t$ as the modulation matrix, the constellation-mapped symbol vector $\mathbf{x} \in \mathbb{C}^{N\times 1}$ is mapped to the discrete-time baseband transmit vector $\mathbf{s}_t$ by

$$\mathbf{s}_t = \mathbf{P}_t \mathbf{x}. \tag{8}$$

A fundamental property of circulant matrices is that they can be diagonalized by the DFT matrix. Let $\mathbf{F}_N$ denote the normalized $N \times N$ DFT matrix. Then, there exists a diagonal matrix $\mathbf{\Lambda}_c$ such that

$$\mathbf{P}_t = \mathbf{F}_N^{\mathrm{H}} \mathbf{\Lambda}_c \mathbf{F}_N, \tag{9}$$

where

$$\mathbf{\Lambda}_c = \mathrm{diag}(\boldsymbol{\lambda}_c), \qquad \boldsymbol{\lambda}_c = \sqrt{N}\, \mathbf{F}_N \mathbf{c}_{\mathrm{Frank}}. \tag{10}$$

Substituting (9) into (8) yields

$$\mathbf{s}_t = \mathbf{F}_N^{\mathrm{H}} \mathbf{\Lambda}_c \mathbf{F}_N \mathbf{x}. \tag{11}$$

Moreover, $\boldsymbol{\lambda}_c$ can be written in a form analogous to (6) as

$$\boldsymbol{\lambda}_c = \mathrm{vec}_{\mathrm{row}}\left(\left(\mathbf{F}_M \,\mathbf{\Pi}\, \mathbf{\Gamma} \right)^{\mathrm{T}} \right), \tag{12}$$

where $\mathbf{F}_M$ denotes the $M \times M$ DFT matrix, $\mathbf{\Gamma}$ is a diagonal unit-modulus matrix, and $\mathbf{\Pi} \in \mathbb{R}^{M\times M}$ is a permutation matrix defined entrywise by

$$[\mathbf{\Pi}]_{i,j} = \begin{cases} 1, & i = (-j) \bmod M, \\ 0, & \text{otherwise}, \end{cases} \qquad i, j \in \{0, 1, \ldots, M-1\}. \tag{13}$$

Note that $\mathbf{\Gamma}$ in (12) and $\mathbf{\Lambda}$ in (6) are both diagonal unit-modulus matrices. However, their diagonal entries are different.

2) Frequency-Shift Realization (Frequency-Shift Modulation): Alternatively, an orthogonal modulation scheme can be constructed by modulating $\mathbf{c}_{\mathrm{Frank}}$ onto different discrete frequencies. Define the discrete frequency-shift operator

$$\mathbf{\Delta}_m \triangleq \mathrm{diag}\left(\left[e^{j\frac{2\pi}{N}0\cdot m}, \; \ldots, \; e^{j\frac{2\pi}{N}(N-1)\cdot m} \right]^{\mathrm{T}} \right), \quad m = 0, 1, \ldots, N-1. \tag{14}$$

Then the set of frequency-shifted waveforms can be written compactly as

$$\begin{aligned} \mathbf{P}_f &= \left[\mathbf{c}_{\mathrm{Frank}}, \; \mathbf{\Delta}_1 \mathbf{c}_{\mathrm{Frank}}, \; \ldots, \; \mathbf{\Delta}_{N-1} \mathbf{c}_{\mathrm{Frank}} \right] \\ &= \mathrm{diag}(\mathbf{c}_{\mathrm{Frank}})\, \mathbf{F}_N^{\mathrm{H}}. \end{aligned} \tag{15}$$

Using $\mathbf{P}_f$ as the modulation matrix, the discrete-time baseband transmit vector $\mathbf{s}_f$ is given by

$$\mathbf{s}_f = \mathbf{P}_f \mathbf{x} = \mathrm{diag}(\mathbf{c}_{\mathrm{Frank}})\, \mathbf{F}_N^{\mathrm{H}} \mathbf{x}. \tag{16}$$

Equations (11) and (16) give the cyclic-shift realization and the frequency-shift realization of the proposed orthogonal modulation based on the PP-Frank waveform, respectively. The two FFT-based realizations are illustrated in Fig. 1. The proposed prototype waveform $\mathbf{c}_{\mathrm{Frank}}$ is handled offline: its time-domain samples are stored, and its N-point DFT coefficients $\boldsymbol{\lambda}_c = \sqrt{N}\mathbf{F}_N \mathbf{c}_{\mathrm{Frank}}$ are precomputed via an N-point FFT, so that no real-time waveform synthesis is required during transmission. In the frequency-shift realization, the constellation-mapped symbol vector $\mathbf{x}$ is first converted to the time domain by an N-point IFFT and then pointwise multiplied by $\mathbf{c}_{\mathrm{Frank}}$, producing the discrete-time baseband transmit

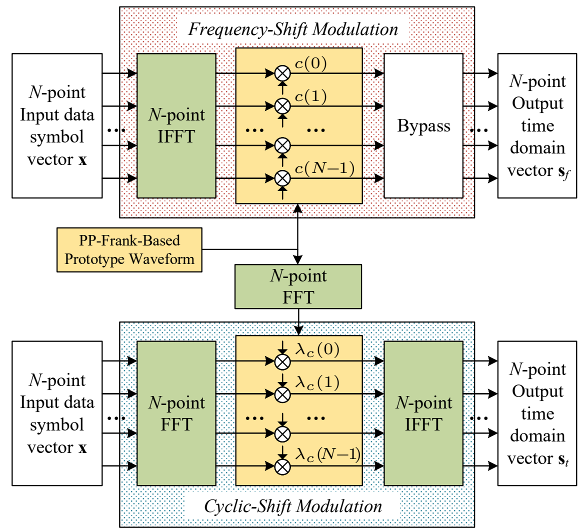

Fig. 1. Two FFT-based realizations of the proposed PP-Frank-sequence-based orthogonal modulation scheme: frequency-shift realization (top) and cyclic-shift realization (bottom).

vector $\mathbf{s}_f = \mathrm{diag}(\mathbf{c}_{\mathrm{Frank}})\mathbf{F}_N^{\mathrm{H}}\mathbf{x}$. In the cyclic-shift realization, the constellation-mapped symbol vector $\mathbf{x}$ is transformed by an N-point FFT, weighted tone-by-tone by the precomputed vector $\boldsymbol{\lambda}_c$, and transformed back by an N-point IFFT, yielding $\mathbf{s}_t = \mathbf{F}_N^{\mathrm{H}}\mathrm{diag}(\boldsymbol{\lambda}_c)\mathbf{F}_N\mathbf{x}$. These two realizations apply the diagonal weighting either in the time domain, through $\mathbf{c}_{\mathrm{Frank}}$, or in the frequency domain, through $\boldsymbol{\lambda}_c$. In both cases, the transmitted symbols are carried by the proposed waveform basis induced by $\mathbf{P}_f$ or $\mathbf{P}_t$.

III. Signal Model and Receiver

In the previous sections, we introduced the proposed PP-Frank-based orthogonal modulation scheme. In this section, we present its use in a practical block-based communication system, including the signal model with cyclic prefix, a baseline MMSE receiver, and an MMSE-initialized iterative MRC receiver for highly doubly selective channels.

A. Signal Model

Let $\mathbf{x} \in \mathbb{C}^{N\times 1}$ denote a block of N data symbols to be transmitted. Using the modulation matrix $\mathbf{P} \in \mathbb{C}^{N\times N}$ defined in (7) or (15), the discrete-time baseband transmit vector becomes

$$\mathbf{s} = \mathbf{P}\mathbf{x}. \tag{17}$$

The received signal model is then

$$\mathbf{y} = \mathbf{H}\mathbf{s} + \mathbf{n} = \mathbf{H}\mathbf{P}\mathbf{x} + \mathbf{n}, \tag{18}$$

where $\mathbf{H} \in \mathbb{C}^{N\times N}$ is the time-varying channel matrix and $\mathbf{n} \in \mathbb{C}^{N\times 1}$ denotes additive noise. We assume $\mathbf{n} \sim \mathcal{CN}(\mathbf{0}, \sigma_n^2\mathbf{I})$ and define $\mathrm{SNR} \triangleq \sigma_x^2/\sigma_n^2$, where $\sigma_x^2 \triangleq \mathbb{E}[|x_k|^2]$. Throughout this paper, the channel matrix is power-normalized such that $\mathbb{E}\left[\mathrm{tr}\left(\mathbf{H}\mathbf{H}^{\mathrm{H}}\right)\right]/N = 1$, so that the above SNR definition is consistent from the transmitter side to the receiver side.

If a cyclic prefix (CP) is inserted, the structure of the time-varying multipath channel matrix $\mathbf{H}$ can be written as

$$[\mathbf{H}]_{n,k} = \begin{cases} h_\ell(n), & \ell = (n-k) \bmod N, \quad 0 \le \ell \le L-1, \\ 0, & \text{otherwise}, \end{cases}$$
$$n, k = 0, 1, \ldots, N-1, \tag{19}$$

where L denotes the maximum delay spread in samples.

It is doubly selective because the delay index ℓ captures multipath dispersion, while the tap coefficient $h_\ell(n)$ varies with the time index n, thereby accounting for Doppler-induced time selectivity within one block. For a time-invariant channel, the resulting channel matrix is circulant due to the CP and can be diagonalized by the DFT matrix, enabling simple one-tap frequency-domain equalization. In doubly selective fading, however, the effective channel matrix is generally non-circulant and cannot be diagonalized in a simple manner [10].

B. MMSE Receiver

We consider linear MMSE detection for the effective model in (18).

$$\hat{\mathbf{x}} = \mathbf{G}_{\mathrm{MMSE}}\mathbf{y}. \tag{20}$$

Let $\mathbf{H}_{\mathrm{eq}} \triangleq \mathbf{HP}$. The MMSE equalizer is

$$\mathbf{G}_{\mathrm{MMSE}} = \left(\mathbf{H}_{\mathrm{eq}}^{\mathrm{H}}\mathbf{H}_{\mathrm{eq}} + \frac{1}{\mathrm{SNR}}\mathbf{I}\right)^{-1}\mathbf{H}_{\mathrm{eq}}^{\mathrm{H}}. \tag{21}$$

For the ith data symbol, the linear MMSE output can be represented as

$$\hat{x}_i = \underbrace{\mathbf{T}_{i,i}x_i}_{\text{Signal}} + \underbrace{\sum_{j\ne i}\mathbf{T}_{i,j}x_j}_{\text{Interference}} + \underbrace{n'_i}_{\text{Noise}}, \tag{22}$$

where $\mathbf{T} \triangleq \mathbf{G}_{\mathrm{MMSE}}\mathbf{H}_{\mathrm{eq}}$ and $\mathbf{n}' \triangleq \mathbf{G}_{\mathrm{MMSE}}\mathbf{n}$.

Here $\mathbf{T}$ characterizes the overall equivalent coupling between the transmitted and received symbols after equalization and waveform transform.

The signal-to-interference-plus-noise ratio (SINR) for the ith data symbol can be expressed as

$$\beta_i = \frac{\left|\mathbf{T}_{i,i}\right|^2\sigma_x^2}{\mathrm{Var}\left(\sum_{j\ne i}\mathbf{T}_{i,j}x_j + n'_i\right)}, \tag{23}$$

where σ_x^2 is the variance of the modulation constellation.

In practice, the central limit theorem is often invoked to approximate the weighted sum of interference terms as a complex Gaussian random variable. Here, we use a simpler expression to compute the SINR. It has been shown in [11] that the SINR for the ith symbol can be written as

$$\beta_i = \frac{\mathbf{T}_{i,i}}{1-\mathbf{T}_{i,i}}. \tag{24}$$

[5] shows that, under typical SNR conditions of conventional communication systems, the BER reaches the theoretical lower bound if and only if all diagonal elements of $\mathbf{T}$ are equal, i.e.,

$$\mathbf{T}_{i,i}^{\mathrm{ideal}} = \bar{T} \triangleq \frac{1}{N}\sum_{k=0}^{N-1}\mathbf{T}_{k,k} = \frac{\mathrm{tr}(\mathbf{T})}{N}, \qquad \forall i, \tag{25}$$

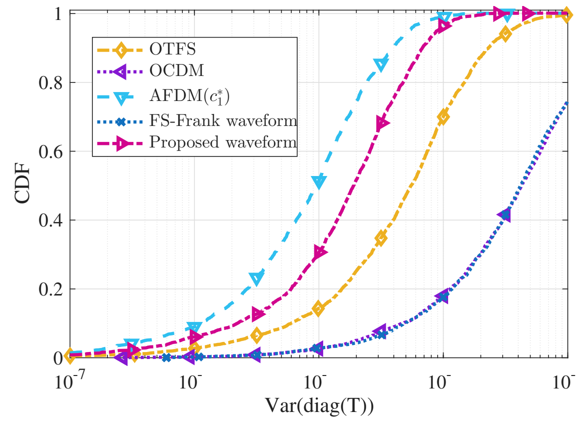

Fig. 2. CDF of the normalized variance of the diagonal entries of the equivalent matrix $\mathbf{T}$ for different waveform schemes.

where $\mathbf{T}_{i,i}^{\mathrm{ideal}}$ denotes the ideal diagonal value of $\mathbf{T}_{i,i}$ that achieves the BER lower bound.

For PP-Frank, different phase patterns induce different effective channels $\mathbf{H}_{\mathrm{eq}} = \mathbf{HP}$ and hence different post-equalization matrices $\mathbf{T}$. This suggests a natural receiver-oriented criterion: choosing $\boldsymbol{\theta}$ to make the diagonal entries of $\mathbf{T}$ more balanced, i.e., to promote more uniform per-symbol post-equalization reliability. In this paper, rather than solving such an optimization problem, we adopt a simple well-spread phase pattern whose entries are approximately uniformly distributed over $[0, 2\pi)$. This choice avoids phase concentration and perturbs the fixed coupling pattern of the FS-Frank waveform in a more even manner, thereby serving as a reasonable non-optimized baseline.

Fig. 2 illustrates the cumulative distribution function (CDF) of the normalized variance of the diagonal elements of the equivalent matrix $\mathbf{T}$ under the Long-Term Evolution (LTE) extended typical urban (ETU) channel model with a terminal speed of $150\ \mathrm{m/s}$ for various waveform schemes. Specifically, the normalized variance is defined as

$$\mathrm{Var_n} \triangleq \frac{\frac{1}{N}\sum_{i=0}^{N-1}\left|\mathbf{T}_{i,i} - \bar{T}\right|^2}{\left|\bar{T}\right|^2}, \qquad \bar{T} \triangleq \frac{1}{N}\,\mathrm{tr}(\mathbf{T}). \tag{26}$$

This metric provides an indirect yet informative indicator of the error-rate performance under MMSE equalization, since a smaller variance of the diagonal elements generally corresponds to a more favorable post-equalization SINR.

In Fig. 2, we compare OTFS, OCDM, the parameter-optimized AFDM, the FS-Frank-based waveform, and the proposed PP-Frank-based waveform. It can be observed that OCDM (as a special case of AFDM) and the FS-Frank-based waveform (as a special case of the proposed waveform) exhibit the same diagonal-element variance, and they also attain the largest diagonal variance among the considered schemes, indicating the least uniform per-symbol equalization quality under MMSE reception. In contrast, AFDM with optimized parameters achieves the smallest diagonal variance, while the proposed waveform yields a variance level between AFDM and OTFS, suggesting that it can provide equalization robustness close to that of parameter-optimized AFDM.

It is worth noting that the proposed waveform already attains a normalized diagonal variance on the order of 10^{-4}, which is close to that of parameter-optimized AFDM. Hence, Fig. 2 suggests only minor BER differences under linear MMSE detection, as also confirmed by the simulations presented later in this paper.

C. Iterative MRC Receiver

Although the MMSE receiver provides an analytically tractable linear benchmark, residual interference remains in highly doubly selective channels. To further improve detection performance, we consider a nonlinear receiver based on interference cancellation and combining. In particular, the iterative MRC receiver studied in this subsection refines the MMSE solution by initializing with the MMSE output and then iteratively performing interference cancellation and MRC to enhance the per-symbol SINR. We adopt MRC, rather than more sophisticated iterative schemes, because it offers low computational complexity while still providing additional gains over linear MMSE detection.

We initialize the iterative detector using the linear MMSE estimate

$$\hat{\mathbf{x}}^{(0)} = \mathbf{G}_{\mathrm{MMSE}}\mathbf{y}. \tag{27}$$

Denote the kth column of $\mathbf{H}_{\mathrm{eq}}$ by $\mathbf{h}_k = \mathbf{H}_{\mathrm{eq}}(:, k)$. At iteration $i \geq 1$, for each symbol index k, we form an interference-cancelled observation

$$\begin{aligned} \tilde{\mathbf{y}}_k^{(i)} &= \mathbf{y} - \mathbf{H}_{\mathrm{eq}}\hat{\mathbf{x}}^{(i-1)} + \mathbf{h}_k \hat{x}_k^{(i-1)} \\ &= \mathbf{h}_k x_k + \mathbf{w}_k^{(i)}, \end{aligned} \tag{28}$$

where $\mathbf{w}_k^{(i)}$ collects the residual interference from other symbols plus noise. We then apply MRC to obtain a soft estimate

$$\hat{s}_k^{(i)} = \frac{\mathbf{h}_k^{\mathrm{H}}\tilde{\mathbf{y}}_k^{(i)}}{\mathbf{h}_k^{\mathrm{H}}\mathbf{h}_k}. \tag{29}$$

Finally, a hard decision is produced by constellation slicing

$$\hat{x}_k^{(i)} = \mathcal{Q}\left(\hat{s}_k^{(i)}\right), \qquad k = 0, 1, \ldots, N-1, \tag{30}$$

where $\mathcal{Q}(\cdot)$ maps to the nearest point in the constellation set.

The above symbol-by-symbol update is repeated for $k = 0, 1, \ldots, N-1$ to complete one full iteration. In this work, the updates within each iteration are carried out sequentially, which corresponds to a Gauss-Seidel-type interference-cancellation schedule. The iterations stop after a prescribed maximum number of iterations I, or earlier if a convergence criterion is met, e.g., $\hat{\mathbf{x}}^{(i)} = \hat{\mathbf{x}}^{(i-1)}$ (no decision changes) or $\|\hat{\mathbf{x}}^{(i)} - \hat{\mathbf{x}}^{(i-1)}\| / \|\hat{\mathbf{x}}^{(i-1)}\|$ falls below a threshold.

D. Complexity Discussion

For transmitter implementation, both realizations can be implemented through FFT operations, leading to a complexity of $\mathcal{O}(N \log N)$. For linear MMSE detection, a direct dense implementation has complexity $\mathcal{O}(N^3)$. Since $\mathbf{P}$ is unitary, however, the dominant solving cost is mainly governed by the structure of the physical channel matrix $\mathbf{H}$ rather than by the waveform basis, so the same sparse-LU-based acceleration can also be applied to PP-Frank, as in existing OTFS and AFDM implementations. For iterative MRC, the straightforward per-iteration complexity is $\mathcal{O}(N^3)$, which can be reduced to $\mathcal{O}(N^2)$ by residual-recursive updating.

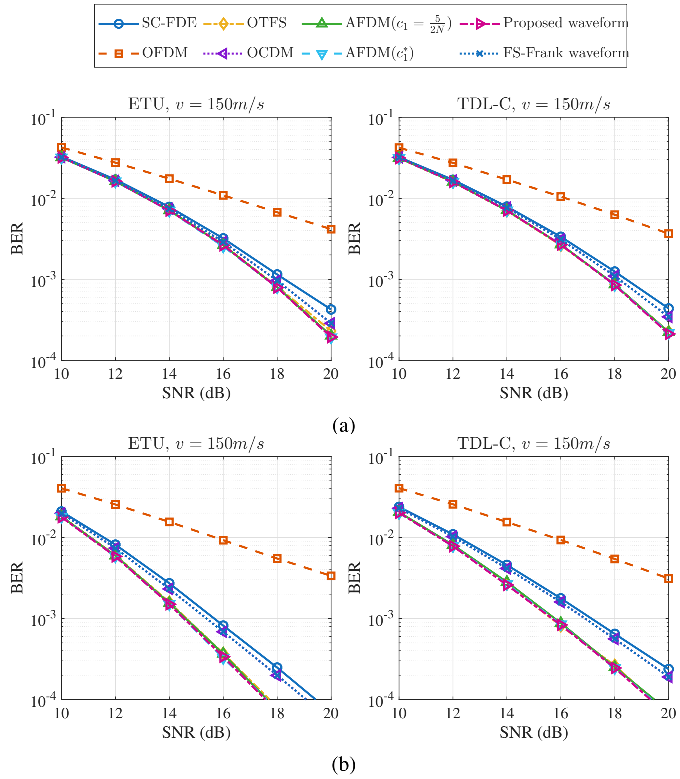

Fig. 3. BER performance comparison of different waveform schemes. (a) MMSE receiver; (b) Iterative MRC receiver.

IV. Performance Simulation and Analysis

In this section, we evaluate and compare the BER performance of SC-FDE, OFDM, OTFS, AFDM, the FS-Frank waveform, and the proposed waveform in different channel environments via numerical simulations. All simulations are carried out under the following assumptions: (a) all waveform schemes adopt block transmission with a block length of $N = 256$, and a CP longer than the maximum delay spread is appended; (b) the carrier frequency is $f_c = 6$ GHz and the subcarrier spacing is $\Delta f = 15$ kHz; (c) QPSK modulation is employed.

The OTFS parameters $M_{\mathrm{OTFS}} = 32$ and $N_{\mathrm{OTFS}} = 8$. The AFDM parameter c_1 are selected according to the optimal values reported in [5] for the corresponding channel conditions. We additionally include two parameters for comparison: $c_1 = \frac{1}{2N}$ (corresponding to OCDM) and other values of c_1. For the proposed waveform, the phase vector θ is chosen such that its entries are approximately uniformly distributed over $[0, 2\pi)$, and the same vector is used for all channel conditions and simulations. The FS-Frank waveform is obtained by setting $\theta = \mathbf{0}$. Both waveforms use the cyclic-shift realization in (11).

Figure 3(a) shows the BER performance of different waveform schemes with an MMSE receiver under various channel conditions. The multipath delay and power profiles follow the LTE ETU channel model and the 3GPP 5G tapped delay

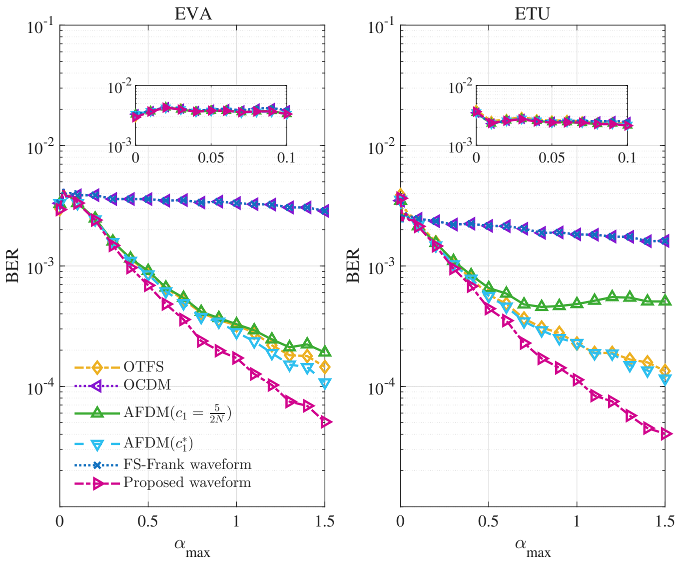

Fig. 4. BER performance of different waveforms versus maximum normalized Doppler $\alpha_{\max}$ under the LTE EVA and ETU channel model with three MRC iterations.

line model C (TDL-C), and the mobile speeds are set to $v = 150$ m/s. The Doppler spectrum follows the classical Jakes model. For channel profiles with non-integer path delays, we adopt a sample-spaced discrete-time approximation in which each path delay is quantized to the nearest upper sampling instant. The same approximation is applied to all compared waveforms for a fair comparison. It can be observed that OFDM exhibits the worst BER performance. Owing to the large delay spreads in both the ETU and TDL-C channels, severe frequency-selective fading arises, which OFDM cannot effectively mitigate. By comparison, the remaining waveforms can mitigate frequency selectivity to different extents. Among them, SC-FDE, OCDM, and the FS-Frank waveform outperform OFDM, yet a noticeable gap to the MMSE lower bound remains. In contrast, OTFS, parameter-optimized AFDM, and the proposed waveform better balance the impacts of time-domain and frequency-domain fading, achieving superior BER performance and approaching the theoretical MMSE lower bound. Figure 3(b) presents the BER performance when the receiver is the iterative MRC receiver with three iterations. Compared with the MMSE receiver, the iterative MRC receiver significantly improves the BER performance.

To illustrate the performance advantage of the proposed waveform in doubly selective channels, Fig. 4 shows the BER of different waveforms as a function of the maximum normalized Doppler $\alpha_{\max} = f_D/\Delta f$ under the LTE extended vehicular A (EVA) and LTE ETU channel models, where f_D is the maximum Doppler frequency and Δf is the subcarrier spacing. In this case, the receiver is the iterative MRC receiver with three iterations, and the average receive SNR is set to 14 dB. [4] considers values of $\alpha_{\max}$ up to 1, whereas here we simulate a wider range $\alpha_{\max} \in [0, 1.5]$. It can be seen that, when the maximum normalized Doppler is small, OTFS, AFDM, and the proposed waveform exhibit similar performance. As the Doppler shift increases, however, the proposed waveform gradually shows a clear performance advantage, which becomes more pronounced with larger $\alpha_{\max}$.

V. Conclusion

This paper proposed a phase-parameterized Frank sequence that preserves the CAZAC property while introducing an additional phase-parameter vector. Based on the proposed sequence, we enlarged the design space within the CAZAC class and proposed two associated orthogonal modulation schemes. Simulation results show that, compared with the FS-Frank construction, the proposed waveform yields more favorable post-equalization behavior under doubly selective fading. When benchmarked against OTFS and AFDM, the proposed waveform achieves comparable BER performance under linear MMSE reception. More importantly, in high-Doppler scenarios and with an iterative MRC receiver, the proposed waveform exhibits a clear performance advantage over OTFS and AFDM, indicating its potential as a waveform candidate for high-mobility links.

Acknowledgment

This work was supported by the Key Program of the National Natural Science Foundation of China under Grant No. U23A20278.

References

[1] 3GPP, “Study on Channel Model for Frequencies from 0.5 to 100 GHz,” 3rd Generation Partnership Project (3GPP), Technical Report TR 38.901 V17.0.0 (Release 17), Mar. 2022, version 17.0.0 (2022-03).

[2] R. Hadani, S. Rakib, M. Tsatsanis, A. Monk, A. J. Goldsmith, A. F. Molisch, and R. Calderbank, “Orthogonal Time Frequency Space Modulation,” in *2017 IEEE Wireless Communications and Networking Conference (WCNC)*, 2017, pp. 1–6.

[3] Z. Wei, W. Yuan, S. Li, J. Yuan, G. Bharatula, R. Hadani, and L. Hanzo, “Orthogonal Time-Frequency Space Modulation: A Promising Next-Generation Waveform,” *IEEE Wireless Communications*, vol. 28, no. 4, pp. 136–144, 2021.

[4] A. Bemani, N. Ksairi, and M. Kountouris, “Affine Frequency Division Multiplexing for Next Generation Wireless Communications,” *IEEE Transactions on Wireless Communications*, vol. 22, no. 11, pp. 8214–8229, 2023.

[5] Z. Li, C. Zhang, G. Song, X. Fang, X. Sha, and D. T. M. Slock, “Chirp Parameter Selection for Affine Frequency Division Multiplexing With MMSE Equalization,” *IEEE Transactions on Communications*, vol. 73, no. 7, pp. 5079–5093, 2025.

[6] X. Ouyang and J. Zhao, “Orthogonal Chirp Division Multiplexing for Coherent Optical Fiber Communications,” *Journal of Lightwave Technology*, vol. 34, no. 18, pp. 4376–4386, 2016.

[7] H. Yin, Y. Tang, A. Bemani, M. Kountouris, Y. Zhou, X. Zhang, Y. Liu, G. Chen, K. Yang, F. Liu, C. Masouros, S. Li, G. Caire, and P. Xiao, “Affine Frequency Division Multiplexing: Extending OFDM for Scenario-Flexibility and Resilience,” *IEEE Wireless Communications*, vol. 32, no. 6, pp. 200–208, 2025.

[8] R. Frank, “Polyphase codes with good nonperiodic correlation properties,” *IEEE Transactions on Information Theory*, vol. 9, no. 1, pp. 43–45, 1963.

[9] D. Chu, “Polyphase codes with good periodic correlation properties,” *IEEE Transactions on Information Theory*, vol. 18, no. 4, pp. 531–532, 1972.

[10] W. Benzine, A. Bemani, N. Ksairi, and D. Slock, “Models, Methods, and Waveforms for Estimation and Prediction of Sparse Time-Varying Channels,” *IEEE Transactions on Wireless Communications*, vol. 25, pp. 9623–9638, 2026.

[11] Y.-P. Lin and S.-M. Phoong, “BER Minimized OFDM Systems With Channel Independent Precoder,” *IEEE Transactions on Signal Processing*, vol. 51, no. 9, pp. 2369–2380, 2003.